Received: 3 July 2021 | Revised: 1 March 2022 | Accepted: 8 March 2022

DOI: 10.1002/ppp.2145

RESEARCH ARTICLE

WILEY

Modeling the role of lateral surface flow in low-relief polygonal tundra

Ahmad Jan[1,2]

[1]Climate Change Science Institute and Environmental Sciences Division, Oak Ridge National Laboratory, Oak Ridge, Tennessee

[2]NOAA-Affiliate, Office of Water Prediction, National Water Center, Tuscaloosa, Alabama

Correspondence
Ahmad Jan, Climate Change Science Institute and Environmental Sciences Division, Oak Ridge National Laboratory, Oak Ridge, TN, USA.
Email: ajkhattak@gmail.com; ahmad.jan@noaa.gov

Funding information
U.S. Department of Energy (Office of Science, Office of Basic Energy Sciences and Energy Efficiency and Renewable Energy, Solar Energy Technology Program); Office of Science; Oak Ridge National Laboratory; Department of Energy, Grant/Award Number: AC05-00OR22725

Abstract

Ice-wedge polygon troughs play an important role in controlling the hydrology of low-relief polygonal tundra regions. Lateral surface flow is confined to troughs only, but it is often neglected in model projections of permafrost thermal hydrology. Recent field and modeling studies have shown that, after rain events, increases in trough water levels are significantly more than the observed precipitation, highlighting the role of lateral surface flow in the polygonal tundra. Therefore, understanding how trough lateral surface flow can influence polygonal tundra thermal hydrology is important, especially under projected changes in temperatures and rainfall in the Arctic regions. Using an integrated cryohydrology model, this study presents plot-scale end-of-century projections of ice-wedge polygon water budget components and active layer thickness with and without trough lateral surface flow under the Representative Concentration Pathway 8.5 scenario. Trough lateral surface flow is incorporated through a newly developed empirical model, evaluated against field measurements. The numerical scenario that includes trough lateral surface flow simulates discharge (outflow from a polygon) and recharge (rain-induced inflow to a polygon trough from upslope areas), while the scenario that does not include trough lateral surface flow ignores recharge. The results show considerable reduction (about 100–150%) in evapotranspiration and discharge in rainy years in the scenarios ignoring trough lateral surface flow, but less effect on soil water storage, in comparison with the scenario with trough lateral surface flow. In addition, the results demonstrate long-term changes (~10–15 cm increase) in active layer thickness when trough lateral surface flow is modeled. This study highlights the importance of including lateral surface flow processes to better understand the long-term thermal and hydrological changes in low-relief polygonal tundra regions under a changing climate.

KEYWORDS
lateral surface flow, permafrost polygonal tundra, projections, simulations, water budget components

1 | INTRODUCTION

Observed and projected warming in the Arctic regions is expected to lead to permafrost degradation.[2–6] Permafrost-affected soils occupy approximately one-quarter of the Northern Hemisphere and store a

significant amount of frozen organic carbon.[7–12] These large carbon stocks are vulnerable to climate-warming-induced permafrost loss and, if decomposed, can be released to the atmosphere.[13–15] Along with warming, climate projections also suggest increases in summer rainfall over the Arctic, though changes in precipitation are uncertain.[16–19] These changes in rainfall together with warming-induced permafrost thaw have the potential to bring substantial hydrological changes to Arctic tundra ecosystems.[20–24] Hydrological changes in those regions have significant implications for water budget components,[25,26] organic matter decomposition, and nutrient export through surface and subsurface drainage,[24,27,28] as well as permafrost carbon feedback.[10,23,24,29–32]

Arctic polygonal tundra landscapes are characterized by a complex mosaic of microtopographic features (center, rim, and trough).[33–36] These microtopographic features are attributed to subsurface ice wedges, which are formed when frozen ground cracks due to thermal contraction.[37–39] These soil thermal contraction and freeze–thaw processes over hundreds to thousands of years tessellate the surface into polygonal patterns. Based on the microtopographic features, these ice-wedge polygons are often classified as low-centered polygons (raised rims and central depression), high-centered polygons (an elevated center that slopes down to troughs), intermediate-centered (slightly degraded low-centered polygon), and flat-centered polygons.[35,40–42] Ice-wedge polygons are widely distributed and can be found in the regions of, for instance, northern Alaska, Siberia, Canada, and Svalbard.[40,43–45]

Under a warming climate, geomorphic changes in ice-wedge polygons, including a transition from low- to high-centered polygons, are expected due to melting of massive wedges of ice beneath the troughs.[46] This evolution of polygon degradation has the potential to develop a well-established drainage network of troughs,[47,48] which could bring substantial thermal hydrological changes to the Arctic regions.[23,28,49,50] Thus, the role of the interconnected network of troughs in controlling surface hydrology in low-relief polygonal tundra landscapes is important.

Numerous studies have shown the importance of microtopographic features in the polygonal landscapes with influence on hydrological processes.[33–35,41,48,51–58] The role of microtopography in controlling subsurface vertical and horizontal water fluxes has been reported in a recent conservative tracer field experiment.[59] Helbig et al.[44] and Boike, Wille, and Abnizova[60] in their field studies have shown that the local hydrological conditions and the summer water balance of the polygonal tundra are strongly influenced by the lateral surface and subsurface flow. Recent field and modeling studies have also reported that, after rain events, the increases in trough water levels are considerably more than the observed rainfall.[1,61,62] Moreover, during summer, water flow from polygon centers through the thawed rims keeps the water table high in polygon troughs.[1,44,63] These studies have highlighted that the dynamics of trough water level: (a) determine the direction of the lateral flow from polygon centers to troughs and vice versa (intrapolygon lateral flow process), and (b) depend heavily on the rain-induced lateral inflow from upslope areas (interpolygon lateral flow process). However, simulating the role of rain-induced trough lateral surface flow in models has not yet been addressed.

To understand the impacts of projected changes in air temperature and precipitation on the thaw-induced transport of decomposed organic matter, quantifying the role of lateral surface and subsurface flow and the associated impacts on water budget components is a prerequisite.[26,44,60] In the polygonal tundra regions, downstream transport of the decomposed nutrients such as carbon and nitrogen, which has implications for stream/river biogeochemistry and water quality,[26,28,64] will be regulated by the drainage network of troughs. Moreover, the antecedent soil moisture conditions will determine: (a) the transport of surface energy fluxes to the permafrost table by altering the soil thermal conductivity, and (b) the rate of the decomposed carbon released as methane (anaerobic conditions) or carbon dioxide (aerobic conditions).[65]

Trough lateral surface flow (hereafter referred to as lateral surface flow; the inflow of water during rainfall events from upslope areas into the polygon troughs) processes are typically neglected in model projections of permafrost thermal hydrology (see, e.g,[66]). In that study,[66] the projections include small-scale transfer of water (among microtopographic locations; center, rim, and trough) but larger scale lateral flows are not modeled. However, due to the key role of the interconnected network of troughs in controlling larger scale surface hydrology, lateral surface flow is an important hydrological process in the polygonal tundra. With rising temperatures and changing rainfall patterns during the 21st century in the Arctic, it is essential to include lateral surface flow processes in models to better understand future hydrological changes in the polygonal tundra regions.

Although there has recently been significant progress in developing integrated cryohydrology models (fully coupled three-dimensional models of permafrost surface and subsurface thermal hydrology),[67–69] the design of numerical experiments is still strongly controlled by the availability of field data, which serve as input for the models. The lack of observed surface hydrological data in the high-latitude regions is a major limiting factor in including lateral surface flow in models. While ignoring lateral surface flow is a reasonable assumption under drier conditions,[26] models consistent with observations have shown that modeling scenarios ignoring lateral surface flow failed to represent measured trough water levels in wetter conditions.[1] As a result, models that do not account for lateral surface flow can result in uncertainties in model evaluation in the current climate,[1] and in analyzing projected impacts of climate change on the polygonal tundra hydrology.

The objective of this work is to mechanistically investigate the role of lateral surface flow in controlling ice-wedge polygons water budget components (i.e., discharge, evapotranspiration, and soil water storage) and active layer thickness (ALT; near-surface seasonally thawed layer). Specifically, using modeling tools, the work evaluates the hypothesis that lateral surface flow is an important process that controls surface discharge, evapotranspiration, and long-term ALT in polygonal tundra landscapes. The hydrology in permafrost-affected soils is subject to a complex interplay of tightly coupled thermal and hydrological processes on the surface and in the subsurface, soil

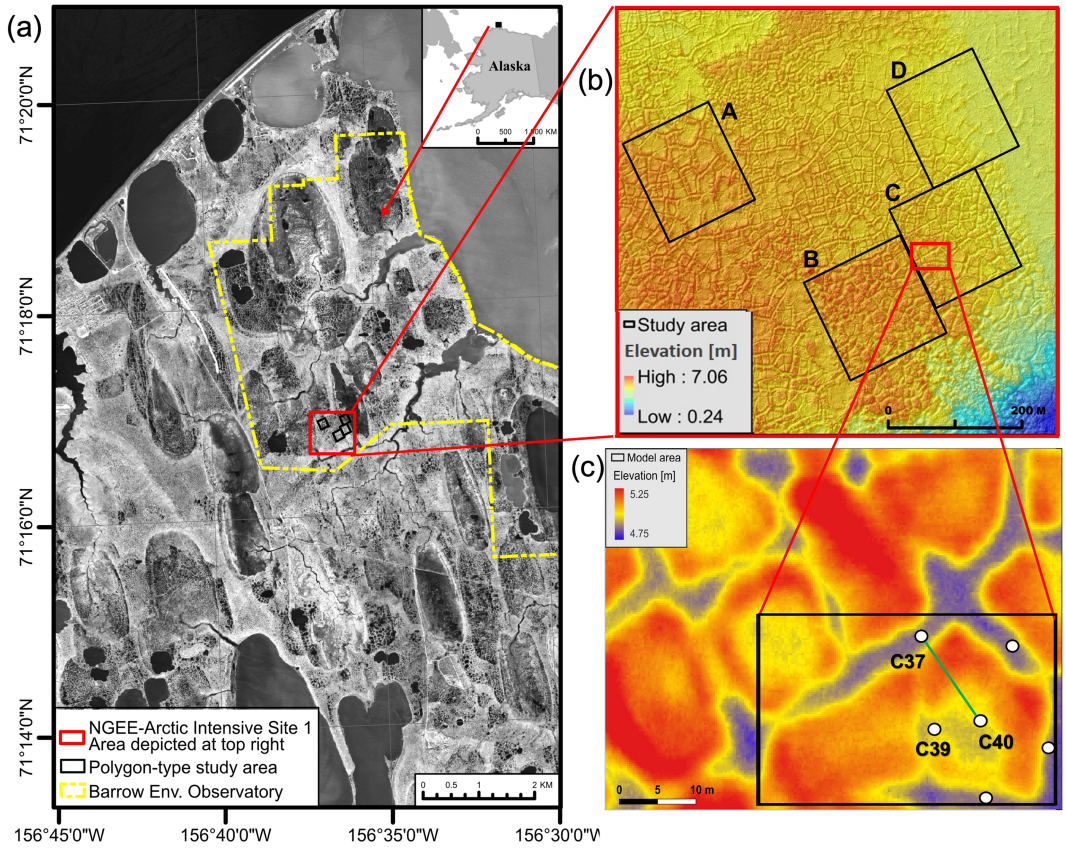

FIGURE 1 Next-generation ecosystem experiments—Arctic field sites at the Barrow environmental observatory. The ice-wedge polygon in area C is outlined in black and the model area is shown by the green transect (c). White dots represent measured water table locations: C37 (trough), C39, and C40 (center). Data from well C37 were used for the evaluation of the empirical trough water table model. The digital elevation model in (b) and (c) is derived from LiDAR measurements[62] [Colour figure can be viewed at wileyonlinelibrary.com]

heterogeneity, surface microtopography, and snow processes. Simulations are essential tools to understand such a complex multiphysics system. Here an integrated cyrohydrology model called Advanced Terrestrial Simulator (ATS)[67] is used to test the above-mentioned hypothesis using a two-dimensional transect from a continuous permafrost site located near Utqiaġvik, Alaska.

2 | METHODS

2.1 | Field site

Observations are taken from the field site of the Next Generation Ecosystem Experiment (NGEE) Arctic project (https://ngee-arctic.ornl.gov) at the Barrow Environmental Observatory (BEO) near Utqiaġvik (formerly Barrow), Alaska (Figure 1). The BEO, a low-relief tundra landscape, is characterized by patterned polygonal ground. The ice-wedge polygons in these patterned grounds are formed due to soil thermal contraction cracks and repeated freezing and thawing of the ground over hundreds to thousands of years.[37–39,46] These polygons are typically classified into high-, low-, intermediate-, and flat-centered polygons based on surface microtopography.[35,40,42] The observed water table at the microtopographic locations (white circles in Figure 1c) and observed transect elevations (green solid line in Figure 1c) came from the NGEE-Arctic study area C, a typical intermediate-centered polygon region. ALT is about 40 (±10) cm at site C. The soil stratigraphy consists of about 2–5 cm of live moss and 6–15 cm of peat overlying silty loam mineral layer and was measured using core samples collected during a field campaign conducted by the NGEE-Arctic field scientists (July 31 – August 3, 2012). In general, permafrost thickness extends to a depth of about 400 m at Barrow.[70] More details about the characteristics of the NGEE Arctic fields sites and polygons are provided in Kumar et al.[34]

2.2 | Model domain

The model domain is a two-dimensional transect from an intermediate-centered polygon in the NGEE-Arctic study area C at the BEO, Alaska. The transect is highlighted with a green solid line in Figure 1(c) and is about 12 m long (Figure 2a). The mesh is constructed in a pie wedge shape, assuming the ice-wedge polygon is radially symmetric (Figure 2b). The bottom boundary of the domain is flat at a depth of 45 m. A horizontal resolution of 25 cm and a variable

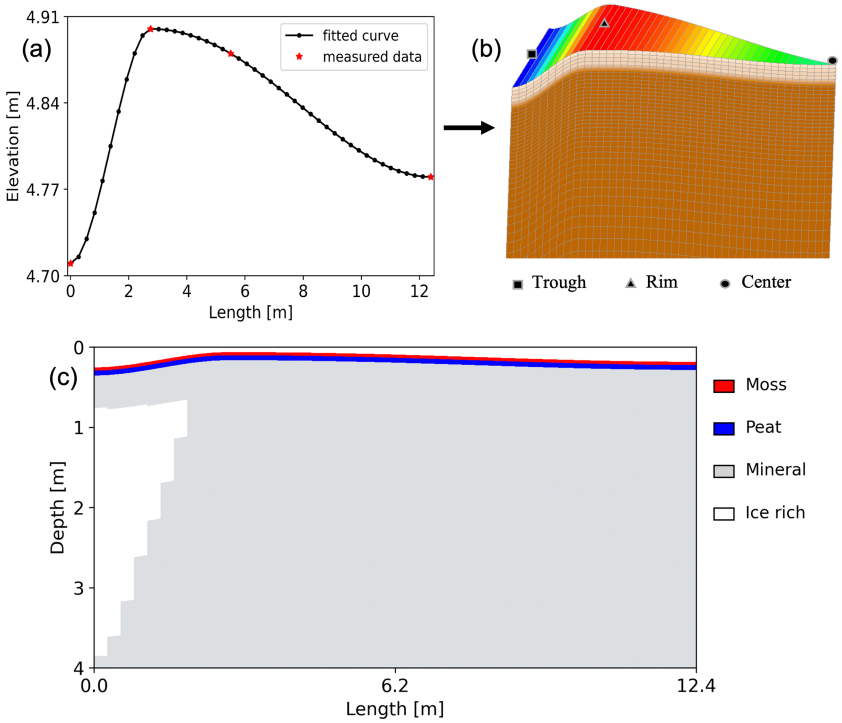

FIGURE 2 Mesh constructed from the observed elevations at the microtopographic locations (trough, rim, and center). (a) Illustration of measured elevations (red asterisks), a spline fit to the observed elevations (black solid line), and spatial resolution (black dots). (b) Pie wedge model for numerical experiments. (c) Side view of the pie wedge model domain. A horizontal resolution of 25 cm and variable vertical resolution is used. The mesh extends to 45 m depth below the trough elevation but is truncated at a depth of ~3.5 m from the surface for visualization purposes [Colour figure can be viewed at wileyonlinelibrary.com]

vertical resolution is used to discretize the domain into 45 × 85 grid cells. The vertical resolution ranges between 2 and 15 cm for the top 10-m domain. A coarse resolution (0.15–5 m) is used for the soil deeper than 10 m. The subsurface is divided into four layers: (a) moss (4 cm), (b) peat (6cm), (c) mineral soil, and (d) ice-rich material. To avoid bottom boundary artifacts, the domain is extended to 45 m depth, but the seasonal thermal signal from the surface does not penetrate deeper than 10–15 m (figure S2 in[71]).

2.3 | Cryohydrology simulator

All modeling scenarios used version 1.0.0 of the ATS[67] configured in cryohydrology mode. The ATS is an integrated surface and subsurface model. The cryohydrology configuration[72] of the ATS couples surface and subsurface thermal hydrology, surface energy balance, and snow distribution modules. The subsurface thermal hydrology module solves a modified form of the Richards equation and energy equation for variably saturated and frozen subsurface soil. The surface thermal hydrology module solves a modified diffusion wave equation for flow and energy. The surface energy balance module is forced with meteorological data, and the snow distribution module uses a phenomenological model (model based on observations) that spatially distributes incoming snow such that microtopographic depressions are filled first. Thus, the ATS permafrost module is a collection of important physical processes, such as lateral surface and subsurface flows, advective heat transport, surface energy balance, cryosuction, and snow processes (compaction, aging, and thermal conduction), needed for simulating process-rich permafrost regions. ATS permafrost modeling capabilities are described in detail in the literature.[41,72–74] For field site C (model area), ATS models were evaluated against observed water table, snow depth, ALT, soil temperatures, and evapotranspiration in multiyear simulations, which showed that the results are very consistent with field observations.[1]

2.4 | Modeling scenarios

Modeling scenarios are categorized as (a) scenarios without lateral surface flow, and (b) a scenario with lateral surface flow. The category without lateral surface flow consists of two scenarios representing discharge (outflow from the trough). The category with lateral surface flow consists of a single scenario that models both discharge (outflow from the polygon trough) and recharge (rain-induced inflow to the polygon trough). That is, the three scenarios differ *only* in how lateral surface flow is represented in the polygon trough. A schematic of water flow lines in the polygon troughs (interpolygon lateral surface flow) and a bidirectional flow between the polygon troughs and center (intrapolygon lateral surface flow) is shown in Figure 3. The scenario with lateral surface flow includes flow due to the white flow lines as well as the black flow lines (single- and double-headed arrows), whereas the scenarios without lateral surface flow do not account for the white flow lines. For the purposes of discussion, the scenarios will be referred to as zero-head and specified-head (without lateral surface flow category) and dynamic-head (with lateral surface flow category) and are summarized in Table 1. The reason for conducting two scenarios in the category without lateral surface flow is to consider extreme cases (boundary conditions) for the discharge. The zero-head scenario represents a free-flow boundary condition (outflow from the trough as water head goes above zero at the datum), and the

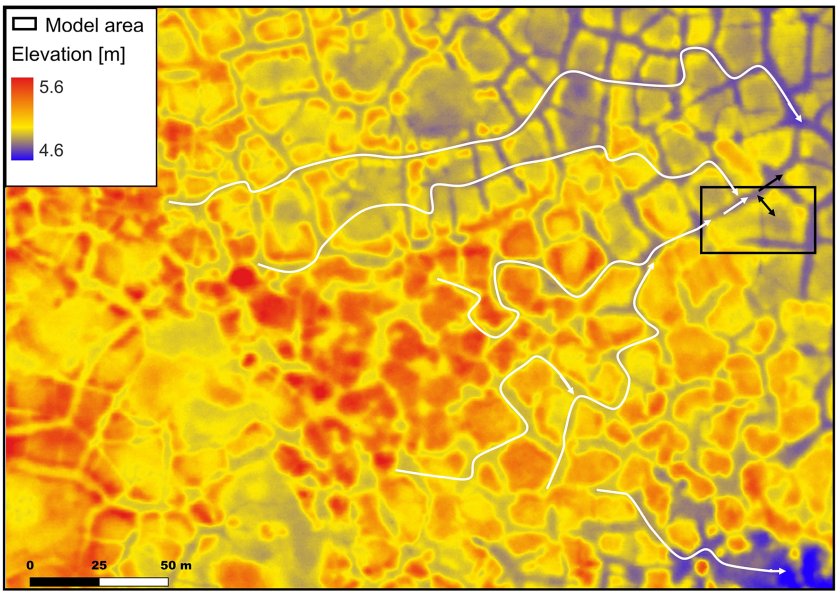

FIGURE 3 Schematic illustrating water flow lines in the ice-wedge polygon troughs. White lines show the larger scale lateral surface flow (interpolygon lateral surface flow). Outflow from the polygon trough is indicated by the black single-headed arrow. The black double-headed arrow indicates a bidirectional flow between polygon troughs and the center (intrapolygon lateral surface flow). Dynamic-head scenario (white and black lines); zero-head and specified-head scenarios (black lines only). The model domain (consistent with Figure 2c) is highlighted in the black rectangle [Colour figure can be viewed at wileyonlinelibrary.com]

TABLE 1 Description of the two categories and modeling scenarios

Category	Scenario	Description
Without lateral surface flow	Zero-head	• No trough inundation • Water freely moves out at the trough • Outflow (discharge) only (black arrows in Figure 3) • Trivial but relatively less realistic
	Specified-head	• Maximum trough inundation • Water drains at the spill point set at 20 cm height • Outflow (discharge) only (black arrows in Figure 3) • Trivial but relatively less realistic
With lateral surface flow	Dynamic-head	• Outflow (discharge) • Inflow (recharge) • Water inflow (white lines in Figure 3) and outflow (black lines in Figure 3) are determined based on an empirical function • Nontrivial but relatively more realistic

specified-head represents a spill point at 20 cm height above the datum (outflow occurs when head at the trough goes above 20 cm of an otherwise closed boundary). It is important to mention that, in the specified-head scenario, the spill point from the datum is set based on the height change from the polygon trough to the rim, which is 20 cm. The dynamic-head scenario, as its name implies, allows us to simulate a dynamic head boundary condition. This boundary condition behaves as discharge or recharge as the simulated water level goes above or below the water level computed by the empirical model (Equation 2), respectively. The zero-head and specified-head scenarios correspond to the maximum and minimum discharge boundary conditions, respectively. While such simplified representations of the lateral surface flow processes are mostly considered in modeling studies,[69] simulating discharge and ignoring recharge makes the representation less realistic.[1] For instance, the zero-head scenario ignores the trough inundation process during the snowmelt period and rain-induced inflow in the post-snowmelt period. Moreover, the specified-head scenario restricts outflow until the trough water level reaches the rim height and neglects the post-snowmelt rain-induced inflow to the polygon trough. In contrast, the dynamic-head scenario is more realistic and leads to an improved representation of lateral surface flow in the polygon troughs.

2.5 | Boundary conditions and model inputs

The surface energy balance equation is subject to meteorological forcing data (air temperature, rain precipitation, snow precipitation, relative humidity, wind speed, and incoming short- and longwave radiation), which serves as the top-surface boundary conditions and provides water/energy fluxes to the subsurface. The temperature at the subsurface bottom boundary is set to −6°C (Romanovsky et al., 2010), and no-flow boundary conditions are used on the vertical sides and at the bottom of the subsurface. In addition to the meteorological forcing data, other inputs to the ATS that are required include porosities, intrinsic permeabilities, soil structure, thermal conductivities, water retention curves, and surface and subsurface thermal and hydrological boundary conditions. The surface and subsurface parameters used in this work are consistent with those of Jan et al.,[1] and are provided in Supporting Information Table S1 for quick reference. The surface flow system is subject to a Dirichlet boundary condition for water head at the polygon trough as explained in subsection 2.4. Note that atmospheric forcing is unchanged among scenarios.

2.6 | Trough lateral surface flow model

The total water budget (the amount of water in a system) can be computed as follows:

$$\Phi = \Phi_0 + P - (ET + \Delta S + Q) \quad (1)$$

Here Φ is the total water budget, Φ_0 is the initial water budget, P is precipitation, ET is evapotranspiration, ΔS is the storage change, and Q is the mass flux (discharge if positive and recharge if negative) that depends on the trough water head (h). In the zero-head and specified-head scenarios, $Q > 0$ if $h > 0$ and $h > 20$ cm, and otherwise zero, respectively. However, in the dynamic-head scenario, the flux Q changes its sign based on the gradient between the simulated head and the prescribed head provided by an empirical model (discussed below). As mentioned earlier, the lateral surface flow in the trough is incorporated through the dynamic-head boundary condition. To that end, a simple empirical model is developed and is expressed mathematically as

$$h_{i+1} = h_i - \alpha t + P^{\beta}, \; t \in T_{i+1}, \; i \geq 0 \quad (2)$$

Here h_i denotes the trough water head (m) at the start of a rain event i, α is the trough flow rate (m day^{-1}), and P denotes precipitation (m). The trough water head, h_0, on the first day of spring (the day when air temperature goes above freezing) is set to 20 cm (height change from the polygon trough to the rim) and is roughly consistent with field observations. T represents the time interval between two consecutive rainfall events on a daily timestep. The variable t (day) corresponds to a day in the time interval T and resets at each rainfall event. The exponent $\beta \geq 0$ depends on the water table height and controls discharge (larger values generate more runoff).

Based on the observed microtopography of ice-wedge polygons, obstructions exist in the polygon troughs and impact runoff during rain events.[41] When the trough water table is below the height of obstruction, rainfall results in trough inundation before initiating runoff. However, rainfall generates runoff when the trough water table is at the height of obstructions. Here, the height of obstructions is assumed to be 0.1 m, half of the rim elevation (4.9 m above sea level) relative to the trough (4.7 m above sea level). Similarly, the trough water level also impacts the outflow rate (discharge). If troughs are inundated, most of the rainwater goes out of the troughs without any restriction to flow when rain occurs. Thus, when the trough water table is higher, the lateral flow rate out of the trough (discharge) is higher and vice versa.

The summer season is split into three hydrological periods: early-snowmelt (air temperature fluctuates around 0°C), snowmelt, and post-snowmelt. The parameters used in the empirical model (Equation 2) for these three periods are summarized in Table 2. A relatively low flow rate in the early-snowmelt period is used to account for snow retardation effects on the trough outflow. Note that the parameter p is always less than 1 (in meters).

Figure 3 compares the trough water table obtained using the empirical model (Equation 2) with the observed water table for the years 2012–2014. While the modeled data fit the observed data reasonably well for the years 2013 and 2014, there is a mismatch between the modeled and the observed data during the 2012 snowmelt period (Figure 4a). This mismatch is due to an artifact in the empirical model. The model only accounts for rain-induced inflow to the polygon trough and ignores snowmelt-induced run-on (water

TABLE 2 Parameters used in the empirical model to simulate rain-induced inflow in the dynamic-head scenario against observed water levels in the polygon trough. Columns correspond to the three hydrological periods in summer, and rows provide values used in the empirical model for the corresponding period. The value 0.1 m in the post-snowmelt column is half of the height change from the polygon trough to the rim representing the height of trough obstructions

	Early-snowmelt	Snowmelt	Post-snowmelt	
			$h > 0.1$ m	$h \leq 0.1$ m
Flow rate α (mm/day)]	1.0	5.0	5.0	2.0
Exponent β (—)	0.0	4.0	4.0	0.75

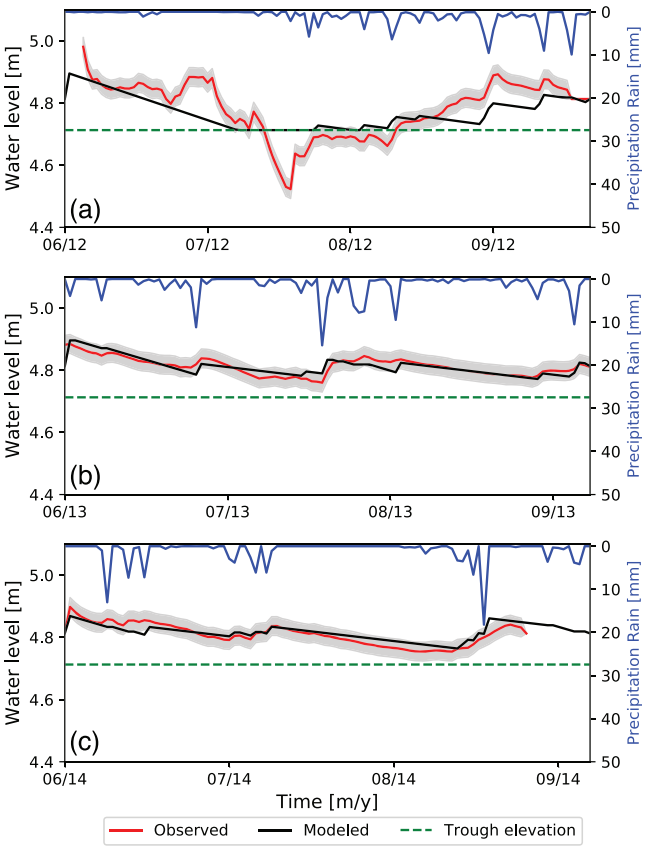

FIGURE 4 Observed and modeled water tables in the ice-wedge polygon trough. The green dotted line is the trough elevation (datum), blue lines are rain precipitation, and rows correspond to different years. Gray shaded curves show the range (±3 cm) of uncertainty in the measured data.[62] [Colour figure can be viewed at wileyonlinelibrary.com]

inflow to the trough from the polygon center and rim and/or from other upslope troughs during the time of snowmelt). Due to a lack of observed snowmelt-induced inflow data, the model assumes that the trough water table decreases linearly during the snowmelt period until rainfall occurs. This limitation can underpredict the observed water table during the snowmelt period, for instance for the 2012 snowmelt period (Figure 4a). While an explicit representation of snowmelt-induced inflow can improve the empirical model, results on an annual basis might not vary considerably. The observed water level dataset is publicly available at the NGEE Arctic data portal.[62]

2.7 | Meteorological forcing data and model initialization

The historical atmospheric data were obtained from Daymet. Daymet provides daily 1×1-km gridded surface data.[75] The projected 100-year linear trend was derived from the Community Earth System Model (CESM) forced with the Representative Concentration Pathway 8.5 (RCP 8.5) emission scenario.[76] The CESM 100-year linear trend is combined with the detrended Daymet data (1985–2015), looping over this period, to obtain daily 100-year projected meteorological data. An empirical model is used to estimate the incoming longwave radiation, details of which can be found in Atchley et al.[73]

The model is spun-up in a multistep procedure: (a) run 1D integrated surface and subsurface simulations, initialized from a 1D frozen column with ice-table close to the surface, using the Daymet forcing data from 1985 repeated 100 times to obtain a cyclical steady-state; (b) map the resulting 1D column to the 2D model domain; and (c) Perform integrated surface and subsurface simulation on the 2D model forced by the Daymet meteorological data from 1986 to 2006 to complete the spin-up process.

3 | RESULTS

The results are discussed from the perspective of hydrological budget components and the long-term ALT in the two categories. For the sake of illustration, time series are smoothed with a 5-year moving average. The mean annual air temperature and mean annual precipitation (snow and rain) are shown in Figure 5(a, b) (solid lines) with dotted lines representing the corresponding linear trends.

3.1 | Discharge

Figure 5(c) illustrates a time series of the mean annual discharge simulated in the three scenarios. Recharge in the dynamic-head scenario is shown by the red solid line (negative Q; below the zero line) in Figure 5(c). The results indicate that the scenarios ignoring lateral surface flow underestimated discharge as compared to the scenario with lateral surface flow (dynamic-head scenario). As expected, a strong correlation between fluctuations in discharge and rainfall in the dynamic-head scenario was observed. In contrast, even in high-rainfall summers, the rainfall–runoff response is minimal towards the end of the century in the scenarios without lateral surface flow. Moreover, irrespective of the numerical scenario, the results show a downward decreasing trend in discharge, and higher early- to midcentury peaks disappeared even for an increasing trend in summer precipitation (Figure 5b and c). This decrease can be explained by the decreasing trend in snow precipitation over the century (gray dotted line in Figure 5b), which strongly affects runoff during the snowmelt period. A time series of annual precipitation (rain and snow) and discharge in early summer (from the first spring day to June 30) and late snowmelt period (July 1 to the first day of fall freeze-up) are shown in the Supporting Information (Figure S1). Recharge (inflow of water to the polygon trough) shows an increasing trend (negative Q in Figure 5c). However, the interannual variations are not as significant as the variations in discharge. For instance, rain precipitation is about 290 and 150 mm in the years 2094 and 2100, respectively, while recharge is

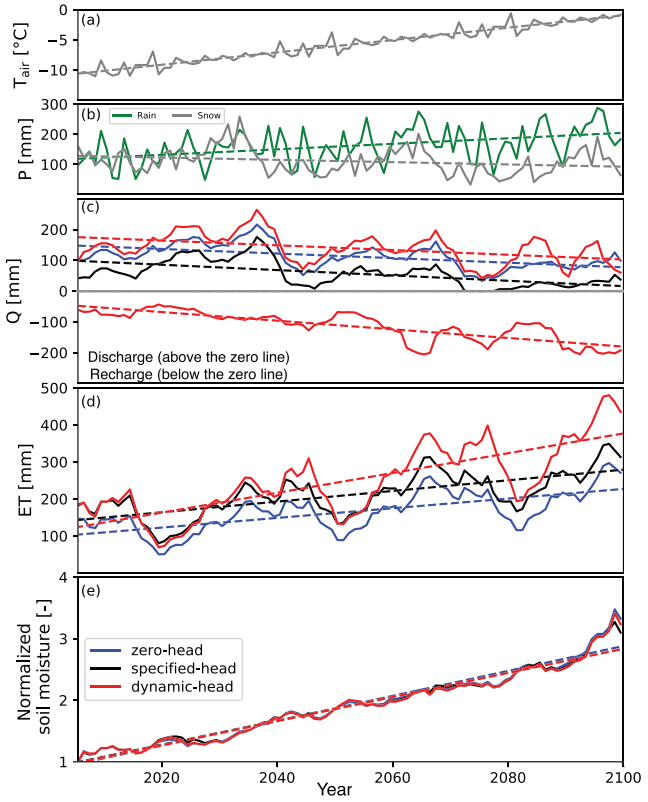

FIGURE 5 Illustrations of the time series of (a) mean annual air temperature (solid line) and a linear trend (dotted line), and (b) mean annual rain and snow precipitations (solid lines) with linear trends (dotted lines). Shown is the simulated: (c) discharge ($Q > 0$) and recharge ($Q < 0$), (d) evapotranspiration (ET), and (e) active layer normalized soil moisture content in the three scenarios. The colors are consistent among panels (c, d, and e). Solid lines (c, d, and e) correspond to the modeling scenarios and dotted lines represent the corresponding linear trends. In (c) the solid red curve above (and below) the zero line (grey) represents discharge (and recharge) in the dynamic-head scenario [Colour figure can be viewed at wileyonlinelibrary.com]

about 200 mm in both years. This is not unexpected because recharge depends strongly on the trough water table before rainfall events. When the trough water table is higher, most of the rainwater goes out of the trough without impacting the recharge.

The height of the spill point in the specified-head scenario caused up to a 100% reduction in the discharge. The spill point is set at 20 cm height above the datum, which allows maximum trough inundation before initiating discharge, thereby causing minimum discharge to occur. During the snowmelt period, as expected, the zero-head scenario generated more discharge than the specified-head scenario, but the maximum discharge was generated in the dynamic-head scenario (Supporting Information Figure S1b). It is worth mentioning that this enhanced discharge in the dynamic-head scenario is not linked to permafrost thaw, as the rate of permafrost loss is roughly similar in all scenarios (Figure S4) except for the post-2090 period. Also, the end of the winter snowpack depth is unchanged among scenarios. Thus, the enhanced discharge in the early summer period in the dynamic-head scenario is the consequence of water inflow to polygon troughs from upslope areas. For instance, the inflow of water to polygon troughs before rainfall keeps the trough inundated and the active layer saturated to some extent, and as rainfall occurs, runoff dominates infiltration due to the limited water storage capacity of the active layer. The active layer is shallow during the early summer period and, if wetter, then even low-intensity rainfall events can generate runoff.

3.2 | Evapotranspiration

To examine the influence of lateral surface flow on evapotranspiration (ET), time series plots of ET for the three scenarios are shown in Figure 5(d). While ET exhibits an increasing trend (dashed lines in Figure 5d) for all modeling scenarios, the rate of increase in the dynamic-head scenario is considerably higher than that in the other scenarios. For instance, in the dynamic-head scenario, ET increased from 150 to 400 mm (∼150% increase) in the period 2080–2100. However, in the scenario without lateral surface flow, the increase in ET is about 50% during the same period. It is interesting to note that the inflow during this period showed no significant variations and is ∼100 mm. The decrease in ET around 2050 and 2080 is due to the sudden drop in the annual average air temperature and the reduction in recharge (Figure 5b and c). Note that the reduction in recharge (solid red line below the zero line in Figure 5c) by 50% during the periods around 2050 and 2080 is the combined effect of the changes in rainfall and height of the trough water table before the rain events. Supporting Information Figure S2 shows that all microtopographic locations (trough, rim, and center) contributed to the increase in ET, but there is significant spatial heterogeneity in ET that is consistent with previous modeling and experimental studies.[1,77,78] The increases in ET are associated with higher air temperatures, increased sublimation (direct evaporation from snow during winter), and increases in summer rainfall over the course of the century. No significant differences in ET were found in the specified-head and dynamic-head scenarios for drier years due to no substantial variations in the net lateral water fluxes, although the zero-head scenario underestimated ET throughout the study period.

3.3 | Soil water storage

To analyze changes in soil water storage, time series plots of the active layer soil moisture content are shown in Figure 5(e). The soil moisture content is averaged over the summer period and normalized by the initial soil moisture content in the summer of 2006. While the projected active layer is about three times wetter than the active layer in the current climate, the rate of increase is fairly uniform among scenarios. The increase in active layer moisture content is due to the permafrost thaw as this increase is consistent with the decrease in permafrost loss and the increase in ALT. While relatively wetter conditions were expected in the dynamic-head scenario due to the addition of extra water to the system, the inflow of water before rainfall events kept the water table higher, which resulted in reduced infiltration during rainfall events. That is, the inflow of water in the dynamic-head scenario contributed to soil water storage, and precipitation is mainly partitioned between discharge and ET. In the scenarios without lateral surface flow, rainfall events contributed more to soil water storage than to ET and discharge. Thereby, the net effect on soil water storage in all scenarios is similar (Supporting Information Figure S3).

3.4 | Active layer thickness

The depth of the active layer, at the trough location, by the end of the study period (the year 2100) for the three scenarios is shown in Figure 6. ALT showed an increase from 45 cm to 155, 148, and 162 cm in the zero-head, specified-head, and dynamic-head scenarios, respectively. This variability shows the long-term effect of lateral

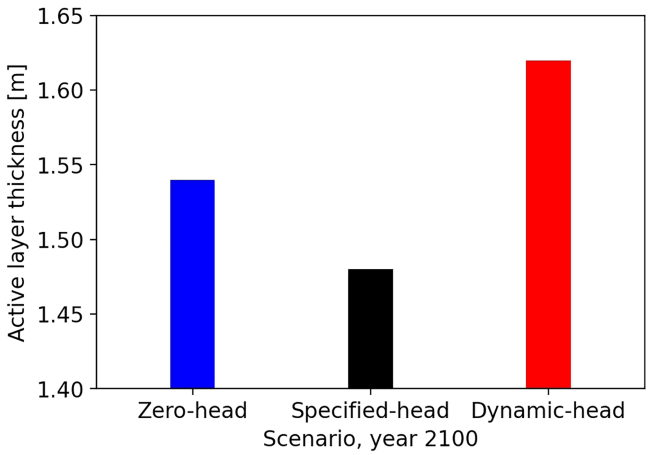

FIGURE 6 Illustration of the active layer thickness at the trough location in the three scenarios for the year 2100 [Colour figure can be viewed at wileyonlinelibrary.com]

surface flow on ALT in polygonal tundra regions. Supporting Information Figure S4 illustrates time series plots of the maximum thaw depth, 5-year moving average, at the three microtopographic locations (trough, rim, and center). The maximum thaw depth varies by microtopographic location of the ice-wedge polygon, illustrating spatial heterogeneity in ALT. However, ALT at the polygon rim and center locations showed less sensitivity to the surface lateral flow in contrast to trough ALT. It is also important to note that, during the period 2040–2090, the trough active layer in the dynamic-head scenario is slightly deeper as compared to the other two scenarios, but the difference is not significant enough to impact hydrological components, especially soil moisture.

4 | SUMMARY AND DISCUSSION

The main objective of this work was to quantify the role of lateral surface flow (rain-induced inflow to polygon troughs from upslope areas) on the thermal hydrology of low-relief polygonal tundra regions. The work was motivated by recent field and modeling studies which have shown that the increases in trough water levels are more than the observed rain precipitation. This suggests that rain precipitation alone is not sufficient to explain trough hydrology, which highlights the important role of lateral surface flow in polygonal tundra landscapes.[1,44,61,63] Plot-scale simulations were performed, using a two-dimensional transect, to study the *long-term* impact of lateral surface flow on the ice-wedge polygon water budget components and ALT under the RCP 8.5 scenario. Although, several field studies have observed lateral flow from polygon centers to troughs through thawed rims and vice versa,[1,44,59,62,63] to the best of my knowledge, this is the first attempt to investigate the role of larger scale lateral surface flow in plot-scale model *projections* on low-relief permafrost thermal hydrology.

The results showed that lateral surface flow has a modest effect on subsurface water storage and short-term ALT. While the results illustrate an increase in the projected moisture content in the active layer under the RCP 8.5 warming climate, the rate of increase is fairly uniform in all scenarios (Supporting Information Figure S3). The presence of impermeable continuous permafrost soil limits the storage and subsurface flow to the active layer,[69,79–81] which strongly impacts the storage capacity of permafrost-affected soils. The variations in ALT among scenarios are not significant apart from for the post-2090 period. This is not unexpected as some of the most dominant factors, such as air temperature, snow precipitation, and soil stratigraphy,[82–84] that control ALT are unchanged among the scenarios. The similar trends in ALT directly influenced the subsurface water storage capacity in all scenarios. It is important to mention that the rate of active layer deepening increased rapidly towards the end of the century in the dynamic-head scenario (Figure S4). This reflects the *long-term* influence of lateral surface flow on ALT, and especially on the thaw depth in the polygon trough, which has significant implications for polygon subsidence. Studies have reported that, under a warming climate, ice-wedge polygons are expected to transition from low- to high-centered due to the melting of massive ice wedges beneath the troughs.[35,46,47,57,85] This evolution of polygon degradation has the potential to develop a well-established drainage network of troughs,[48] which has implications for trough hydrology, polygon water budget components, and downstream nutrient export.[36] While studies have shown a strong correlation between air temperature and summer thaw depth,[20,46,79,86,87] the changes in thaw depth found here are due to lateral surface flow as air temperatures are unchanged among the scenarios.

Among the hydrological budget components, changes in ET are more pronounced than changes in the other components in the three scenarios. Due to no significant variations in the net lateral water fluxes, no major changes in ET were found among scenarios for drier years (mean annual precipitation less than the average). However, in wetter years, ET almost doubled in the dynamic-head scenario. For most of the years, annual average ET exceeds total precipitation, which is consistent with observations in the polygonal tundra.[44] While higher air temperatures are expected to increase potential ET (Andresen et al, 2020), the availability of water in the active layer will determine the actual ET. The representation of trough hydrology in models can strongly impact the actual ET. For instance, the zero-head scenario resulted in reduced projected ET in comparison to the specified-head scenario. This is due to the partitioning of rainfall and snowmelt water into lateral outflow (i.e., discharge) and vertical flow (i.e., infiltration and ET). Ignoring restrictions to flow in the troughs, such as the zero-head scenario, led to enhanced lateral outflow from the trough, which negatively impacted ET. In contrast, considerable restrictions to flow, such as the high spill point in the specified-head scenario, can significantly diminish outflow and intensify ET. This is consistent with field and modeling studies for permafrost regions.[1,77,89] In the dynamic-head scenario, accounting for rain-induced inflow and modeling the hydrodynamics of polygon troughs resulted in enhanced discharge during the snowmelt period and increased ET. This enhanced discharge has implications for the transport of dissolved organic matter.[24,28,88] The three microtopographic experienced considerable evaporative cooling (heat loss to the atmosphere through evaporation) (see Supporting Information Figure S2). The importance of evaporative cooling, an important nonconductive heat flux, in cooling soil has been reported in previous studies (see, e.g.,[6,89–91]). The results of this study show wetter soil conditions, enhanced ET, and reduced discharge by the end of the century under the RCP 8.5 scenario. In conclusion, the present study highlights the importance of modeling lateral surface flow in simulations for reliable *long-term* projections of water budget components and ALT in the polygonal tundra.

Although the results are limited to an intermediate-centered polygon with static microtopography, the insights provided here will help to advance the current and future understanding of permafrost thermal and hydrological processes in low-gradient polygonal tundra regions. Further research considering dynamic microtopography, and thaw-induced subsidence of raised rims, for the evolution of ice-wedge polygons are needed to better understand the impact of lateral surface flow processes on the thermal hydrology of polygonal tundra.

However, this will require additional observational hydrological data for different types of polygons across a watershed and for a longer period to capture different hydrological conditions.

ACKNOWLEDGEMENTS

I thank Associate Editor Nicolas Jelinski, the two anonymous reviewers, Scott Painter, and Alexandra Hamm whose comments and suggestions greatly helped to improve the manuscript. This research used resources of the Compute and Data Environment for Science (CADES) at the Oak Ridge National Laboratory, which is supported by the Office of Science of the U.S. Department of Energy under Contract No. DE-AC05-00OR22725. The author also thank the Next-Generation Ecosystem Experiments Arctic (NGEE-Arctic) project for providing data that have contributed to the results reported in this paper. The NGEE Arctic project is supported by the Office of Biological and Environmental Research in the U.S. Department of Energy's Office of Science.

CODE/DATA AVAILABILITY

The Advanced Terrestrial Simulator (ATS)[67] is open source under the BSD 3-clause license, and is publicly available at https://github.com/amanzi/ats. Simulations were carried out using version 1.0.0. The data that support the findings of this study are available from the corresponding author upon reasonable request. In addition, the forcing data, model input files, and jupyter notebooks for pre- and post-processing will also be made publicly available through a long-term data archive.

DATA AVAILABILITY STATEMENT

The data that support the findings of this study are available from the corresponding author upon reasonable request.

ORCID

Ahmad Jan https://orcid.org/0000-0003-2781-7857

REFERENCES

1. Jan A, Coon ET, Painter SL. Evaluating Integrated Surface/Subsurface Permafrost Thermal Hydrology Models in ATS (v0.88) against Observations from a Polygonal Tundra Site. *Geosci Model Dev*. 2020;13(5):2259-2276. doi:10.5194/gmd-13-2259-2020
2. Batir JF, Hornbach MJ, Blackwell DD. Ten Years of Measurements and Modeling of Soil Temperature Changes and Their Effects on Permafrost in Northwestern Alaska. *Global Planet Change*. 2017;148(January):55-71. doi:10.1016/j.gloplacha.2016.11.009
3. Farquharson LM, Romanovsky VE, Cable WL, Walker DA, Kokelj SV, Nicolsky D. Climate Change Drives Widespread and Rapid Thermokarst Development in Very Cold Permafrost in the Canadian High Arctic. *Geophys Res Lett*. 2019;46(12):6681-6689. doi:10.1029/2019GL082187
4. Lachenbruch AH, Marshall BV. Changing Climate: Geothermal Evidence from Permafrost in the Alaskan Arctic. *Science (New York, NY)*. 1986;234(4777):689-696. doi:10.1126/science.234.4777.689
5. Romanovsky V, Burgess M, Smith S, Yoshikawa K, Brown J. Permafrost Temperature Records: Indicators of Climate Change. *Eos, Trans Am Geophys Union*. 2002;83(50):589-594. doi:10.1029/2002EO000402
6. Wu Q, Zhang T. Recent Permafrost Warming on the Qinghai-Tibetan Plateau. *J Geophys Res Atmos*. 2008;113(D13):D13108. doi:10.1029/2007JD009539
7. Brown J, Ferrians OJ Jr, Alan Heginbottom J, Melnikov ES. *Circum-Arctic Map of Permafrost and Ground-Ice Conditions*. VA: US Geological Survey Reston; 1997.
8. Hugelius G, Strauss J, Zubrzycki S, et al. Estimated Stocks of Circumpolar Permafrost Carbon with Quantified Uncertainty Ranges and Identified Data Gaps. *Biogeosciences*. 2014;11(23):6573-6593. doi:10.5194/bg-11-6573-2014
9. Jorgenson MT, Racine CH, Walters JC, Osterkamp TE. Permafrost Degradation and Ecological Changes Associated with a WarmingClimate in Central Alaska. *Clim Change*. 2001;48(4):551-579. doi:10.1023/A:1005667424292
10. Schuur EAG, McGuire AD, Schädel C, et al. Climate Change and the Permafrost Carbon Feedback. *Nature*. 2015;520(7546):171-179. doi:10.1038/nature14338
11. Tarnocai C, Canadell JG, Schuur EAG, Kuhry P, Mazhitova G, Zimov S. Soil Organic Carbon Pools in the Northern Circumpolar Permafrost Region. *Glob Biogeochem Cycles*. 2009;23(2):GB2023. doi:10.1029/2008GB003327
12. Zimov SA, Schuur EAG, Chapin FS. Permafrost and the Global Carbon Budget. *Science*. 2006;312(5780):1612-1613. doi:10.1126/science.1128908
13. Burke EJ, Jones CD, Koven CD. Estimating the Permafrost-Carbon Climate Response in the CMIP5 Climate Models Using a Simplified Approach. *J Climate*. 2013;26(14):4897-4909. doi:10.1175/JCLI-D-12-00550.1
14. Koven CD, Ringeval B, Friedlingstein P, et al. Permafrost Carbon-Climate Feedbacks Accelerate Global Warming. *Proc Natl Acad Sci U S a*. 2011;108(36):14769-14774. doi:10.1073/pnas.1103910108
15. Turetsky MR, Abbott BW, Jones MC, et al. Carbon Release through Abrupt Permafrost Thaw. *Nat Geosci*. 2020;13(2):138-143. doi:10.1038/s41561-019-0526-0
16. AMAP. 2017. "Snow, Water, Ice and Permafrost. Summary for Policy-Makers."
17. Bintanja R. The Impact of Arctic Warming on Increased Rainfall. *Sci Rep*. 2018;8(1):1-6. doi:10.1038/s41598-018-34450-3
18. Bintanja R, Andry O. Towards a Rain-Dominated Arctic. *Nature Climate Change*. 2017;7(4):263-267. doi:10.1038/nclimate3240
19. Bintanja R, Selten FM. Future Increases in Arctic Precipitation Linked to Local Evaporation and Sea-Ice Retreat. *Nature*. 2014;509(7501):479-482. doi:10.1038/nature13259
20. Evans SG, Ge S. Contrasting Hydrogeologic Responses to Warming in Permafrost and Seasonally Frozen Ground Hillslopes. *Geophys Res Lett*. 2017;44(4):1803-1813. doi:10.1002/2016GL072009
21. Michel FA, Van Everdingen RO. Changes in Hydrogeologic Regimes in Permafrost Regions Due to Climatic Change. *Permafr Periglac Process*. 1994;5(3):191-195. doi:10.1002/ppp.3430050308
22. Osterkamp TE. Response of Alaskan Permafrost to Climate. In: *In Proceedings of the Fourth International Conference on Permafrost*. 2:145-52. Washington, D.C.: National Academy Press; 1983.
23. Pachauri RK, Allen MR, Barros VR, et al. 2014. *Climate Change 2014: Synthesis Report. Contribution of Working Groups I, II and III to the Fifth Assessment Report of the Intergovernmental Panel on Climate Change*. Edited by R. K. Pachauri and L. Meyer. EPIC3Geneva, Switzerland, IPCC, *151 p., Pp. 151, ISBN: 978–92–9169-143-2*. Geneva, Switzerland: IPCC. https://epic.awi.de/id/eprint/37530/
24. Walvoord MA, Kurylyk BL. Hydrologic Impacts of Thawing Permafrost-A Review. *Vadose Zone J*. 2016;15(6):1-20. doi:10.2136/vzj2016.01.0010
25. Woo M-k. Consequences of Climatic Change for Hydrology in Permafrost Zones. *J Cold Regions Eng*. 1990;4(1):15-20. doi:10.1061/(ASCE)0887-381X(1990)4:1(15)

26. Koch JC, Jorgenson MT, Wickland KP, Kanevskiy M, Striegl R. Ice Wedge Degradation and Stabilization Impact Water Budgets and Nutrient Cycling in Arctic Trough Ponds. *J Geophys Res Biogeo*. 2018; 123(8):2604-2616. doi:10.1029/2018JG004528
27. Schuur EAG, Bockheim J, Canadell JG, et al. Vulnerability of Permafrost Carbon to Climate Change: Implications for the Global Carbon Cycle. *Bioscience*. 2008;58(8):701-714. doi:10.1641/B580807
28. Walvoord MA, Striegl RG. Increased Groundwater to Stream Discharge from Permafrost Thawing in the Yukon River Basin: Potential Impacts on Lateral Export of Carbon and Nitrogen. *Geophys Res Lett*. 2007;34(12):L12402. doi:10.1029/2007GL030216
29. ACIA, Eds. 2005. "Arctic Climate Impact Assessment." *ACIA Overview* Report
30. Berghuijs WR, Woods RA, Hrachowitz M. A Precipitation Shift from Snow towards Rain Leads to a Decrease in Streamflow. *Nature Climate Change*. 2014;4(7):583-586. doi:10.1038/nclimate2246
31. Nilsson C, Polvi LE, Lind L. Extreme Events in Streams and Rivers in Arctic and Subarctic Regions in an Uncertain Future. *Freshwater Biology*. 2015;60(12):2535-2546. doi:10.1111/fwb.12477
32. Schädel C, Bader MF, Schuur EAG, et al. Potential Carbon Emissions Dominated by Carbon Dioxide from Thawed Permafrost Soils. *Nature Climate Change*. 2016;6(10):950-953. doi:10.1038/nclimate3054
33. Abolt CJ, Young MH, Atchley AL, Harp DR. Microtopographic Control on the Ground Thermal Regime in Ice Wedge Polygons. *Cryosphere*. 2018;12(6):1957-1968. doi:10.5194/tc-12-1957-2018
34. Kumar J, Collier N, Bisht G, et al. Modeling the Spatiotemporal Variability in Subsurface Thermal Regimes across a Low-Relief Polygonal Tundra Landscape. *Cryosphere*. 2016;10(5):2241-2274. doi:10.5194/tc-10-2241-2016
35. Liljedahl AK, Hinzman LD, Schulla J. Ice-Wedge Polygon Type Controls Low-Gradient Watershed-Scale Hydrology. In: *In Proceedings of the Tenth International Conference on Permafrost*, 1:231–36. Salekhard, Russia: The Northern Publisher; 2012.
36. Newman BD, Throckmorton HM, Graham DE, et al. Microtopographic and Depth Controls on Active Layer Chemistry in Arctic Polygonal Ground. *Geophys Res Lett*. 2015;42(6):1808-1817. doi:10.1002/2014GL062804
37. Greene, G. W. 1963. "Contraction Theory of Ice-Wedge Polygons: A Qualitative Discussion." In *Permafrost International Conference: Proceedings*. Lafayette, Indiana, USA.
38. Lachenbruch AH. Mechanics of Thermal Contraction Cracks and Ice-Wedge Polygons in Permafrost. *GSA Special Papers*. 70. Geological Society of America. 1962. doi:10.1130/SPE70-p1
39. Mackay JR. Some Observations on the Growth and Deformation of Epigenetic, Syngenetic and Anti-Syngenetic Ice Wedges. *Permafr Periglac Process*. 1990;1(1):15-29. doi:10.1002/ppp.3430010104
40. Black, Robert F. 1982. "Ice-Wedge Polygons of Northern Alaska." In *Glacial Geomorphology*, edited by Donald R. Coates, 247–275. Dordrecht: Springer Netherlands. 10.1007/978-94-011-6491-7_9.
41. Jan A, Coon ET, Graham JD, Painter SL. A Subgrid Approach for Modeling Microtopography Effects on Overland Flow. *Water Resour Res*. 2018a;54(9):6153-6167. doi:10.1029/2017WR021898
42. Oechel WC, Vourlitis GL, Hastings SJ, Bochkarev SA. Change in Arctic CO2Flux Over Two Decades: Effects of Climate Change at Barrow, Alaska. *Ecol Appl*. 1995;5(3):846-855. doi:10.2307/1941992
43. Fritz M, Wolter J, Rudaya N, et al. Holocene Ice-Wedge Polygon Development in Northern Yukon Permafrost Peatlands (Canada). *Quat Sci Rev*, Special Issue: PAST Gateways (Palaeo-Arctic Spatial and Temporal Gateways). 2016;147(September):279-297. doi:10.1016/j.quascirev.2016.02.008
44. Helbig M, Boike J, Langer M, Schreiber P, Runkle BRK, Kutzbach L. Spatial and Seasonal Variability of Polygonal Tundra Water Balance: Lena River Delta, Northern Siberia (Russia). *Hydrgeol J*. 2013;21(1): 133-147. doi:10.1007/s10040-012-0933-4
45. Matsuoka N, Christiansen HH, Watanabe T. Ice-Wedge Polygon Dynamics in Svalbard: Lessons from a Decade of Automated Multi-Sensor Monitoring. *Permafr Periglac Process*. 2018;29(3):210-227. doi:10.1002/ppp.1985
46. Jorgenson MT, Shur YL, Pullman ER. Abrupt Increase in Permafrost Degradation in Arctic Alaska. *Geophys Res Lett*. 2006;33(2):L02503. doi:10.1029/2005GL024960
47. Rettelbach T, Langer M, Nitze I, et al. A Quantitative Graph-Based Approach to Monitoring Ice-Wedge Trough Dynamics in Polygonal Permafrost Landscapes. *Remote Sens*. 2021;13(16):3098-3121. doi:10.3390/rs13163098
48. Liljedahl AK, Boike J, Daanen RP, et al. Pan-Arctic Ice-Wedge Degradation in Warming Permafrost and Its Influence on Tundra Hydrology. *Nat Geosci*. 2016;9(4):312-318. doi:10.1038/ngeo2674
49. Koven CD, Riley WJ, Stern A. Analysis of Permafrost Thermal Dynamics and Response to Climate Change in the CMIP5 Earth System Models. *J Climate*. 2013;26(6):1877-1900. doi:10.1175/JCLI-D-12-00228.1
50. Lyon SW, Destouni G, Giesler R, et al. Estimation of Permafrost Thawing Rates in a Sub-Arctic Catchment Using Recession Flow Analysis. *Hydrol Earth Syst Sci*. 2009;13(5):595-604. doi:10.5194/hess-13-595-2009
51. Abolt CJ, Young MH. High-Resolution Mapping of Spatial Heterogeneity in Ice Wedge Polygon Geomorphology near Prudhoe Bay, Alaska. *SciData*. 2020;7:87. doi:10.1038/s41597-020-0423-9
52. Engstrom R, Hope A, Kwon H, Stow D, Zamolodchikov D. Spatial Distribution of near Surface Soil Moisture and Its Relationship to Microtopography in the Alaskan Arctic Coastal Plain. *Hydrol Res*. 2005; 36(3):219-234. doi:10.2166/nh.2005.0016
53. Higgins KL, Garon-Labrecque M-È. Fine-Scale Influences on Thaw Depth in a Forested Peat Plateau Landscape in the Northwest Territories, Canada: Vegetation Trumps Microtopography. *Permafr Periglac Process*. 2018;29(1):60-70. doi:10.1002/ppp.1961
54. Witharana C, Bhuiyan MAE, Liljedahl AK, et al. An Object-Based Approach for Mapping Tundra Ice-Wedge Polygon Troughs from Very High Spatial Resolution Optical Satellite Imagery. *Remote Sens*. 2021;13(4):558-579. doi:10.3390/rs13040558
55. Bisht G, Riley WJ, Wainwright HM, Dafflon B, Yuan F, Romanovsky VE. Impacts of Microtopographic Snow Redistribution and Lateral Subsurface Processes on Hydrologic and Thermal States in an Arctic Polygonal Ground Ecosystem: A Case Study Using ELM-3D v1.0. *Geosci Model Dev*. 2018;11(1):61-76. doi:10.5194/gmd-11-61-2018
56. Grant RF, Mekonnen ZA, Riley WJ, Arora B, Torn MS. Mathematical Modelling of Arctic Polygonal Tundra with Ecosys: 2. Microtopography Determines How CO2 and CH4 Exchange Responds to Changes in Temperature and Precipitation. *J Geophys Res Biogeo*. 2017;122(12):3174-3187. doi:10.1002/2017JG004037
57. Nitzbon J, Langer M, Westermann S, Martin L, Aas KS, Boike J. Pathways of Ice-Wedge Degradation in Polygonal Tundra under Different Hydrological Conditions. *Cryosphere*. 2019;13(4):1089-1123. doi:10.5194/tc-13-1089-2019
58. Zhang W, Witharana C, Liljedahl A, Kanevskiy M. Deep Convolutional Neural Networks for Automated Characterization of Arctic Ice-Wedge Polygons in Very High Spatial Resolution Aerial Imagery. *Remote Sens*. 2018;10(9):1487-1517. doi:10.3390/rs10091487
59. Wales NA, Gomez-Velez JD, Newman BD, et al. Understanding the Relative Importance of Vertical and Horizontal Flow in Ice-Wedge Polygons. *Hydrol Earth Syst Sci*. 2020;24(3):1109-1129. doi:10.5194/hess-24-1109-2020
60. Boike J, Wille C, Abnizova A. Climatology and Summer Energy and Water Balance of Polygonal Tundra in the Lena River Delta, Siberia. *Eur J Vasc Endovasc Surg*. 2008;113(G3):G03025. doi:10.1029/2007JG000540

61. Harp DR, Zlotnik V, Abolt CJ, et al. New Insights into the Drainage of Inundated Ice-Wedge Polygons Using Fundamental Hydrologic Principles. *Cryosphere*. 2021;15(8):4005-4029. doi:10.5194/tc-15-4005-2021
62. Liljedahl AK, Wilson C. Ground Water Levels for NGEE Areas A, B, C and D, Barrow, Alaska, 2012–2014. Next Generation Ecosystem Experiments Arctic Data Collection, Oak Ridge National Laboratory, U.S. Department of Energy, Oak Ridge, Tennessee, USA. Dataset accessed on September, 2018. 2016. doi:10.5440/1183767.
63. Koch JC, Gurney K, Wipfli MS. Morphology-Dependent Water Budgets and Nutrient Fluxes in Arctic Thaw Ponds. *Permafrost and Periglacial Processes*. 2014;25(2):79-93. doi:10.1002/ppp.1804
64. Frey KE, McClelland JW. Impacts of Permafrost Degradation on Arctic River Biogeochemistry. *Hydrol Process*. 2009;23(1):169-182. doi:10.1002/hyp.7196
65. Lee H, Schuur EAG, Inglett KS, Lavoie M, Chanton JP. The Rate of Permafrost Carbon Release under Aerobic and Anaerobic Conditions and Its Potential Effects on Climate. *Glob Chang Biol*. 2012;18(2):515-527. doi:10.1111/j.1365-2486.2011.02519.x
66. Nitzbon J, Westermann S, Langer M, et al. Fast Response of Cold Ice-Rich Permafrost in Northeast Siberia to a Warming Climate. *Nat Commun*. 2020;11:2201. doi:10.1038/s41467-020-15725-8
67. Coon E, Svyatsky D, Jan A, et al. Advanced Terrestrial Simulator. Computer Software. https://github.com/amanzi/ats. USDOE Office of Science (SC), Biological and Environmental Research (BER) (SC-23). 10 Sep. 2019. Web. doi:10.11578/dc.20190911.1
68. Endrizzi S, Gruber S, Dall'Amico M, Rigon R. GEOtop 2.0: Simulating the Combined Energy and Water Balance at and below the Land Surface Accounting for Soil Freezing, Snow Cover and Terrain Effects. *Geosci Model Dev*. 2014;7(6):2831-2857. doi:10.5194/gmd-7-2831-2014
69. Lamontagne-Hallé P, McKenzie JM, Kurylyk BL, Molson J, Lyon LN. Guidelines for Cold-Regions Groundwater Numerical Modeling. *WIREs Water*. 2020;7(6):e1467. doi:10.1002/wat2.1467
70. Lachenbruch AH, Sass JH, Lawver LA, et al. Temperature and Depth of Permafrost on the Arctic Slope of Alaska, in Gryc, George, Ed., U.S. Geological Survey Professional Paper 1399: 1988. 645-56.
71. Jan A, Painter SL. Permafrost Thermal Conditions Are Sensitive to Shifts in Snow Timing. *Environ Res Lett*. 2020;15(8):084026. doi:10.1088/1748-9326/ab8ec4
72. Painter SL, Coon ET, Atchley AL, et al. Integrated Surface/Subsurface Permafrost Thermal Hydrology: Model Formulation and Proof-of-Concept Simulations. *Water Resour Res*. 2016;52(8):6062-6077. doi:10.1002/2015WR018427
73. Atchley AL, Painter SL, Harp DR, et al. Using Field Observations to Inform Thermal Hydrology Models of Permafrost Dynamics with ATS (v0. 83). *Geosci Model Dev*. 2015;8(9):2701-2722. doi:10.5194/gmd-8-2701-2015
74. Jan A, Coon ET, Painter SL, Garimella R, David J, Moulton. An Intermediate-Scale Model for Thermal Hydrology in Low-Relief Permafrost-Affected Landscapes. *Comput Geosci*. 2018b;22(1):163-177. doi:10.1007/s10596-017-9679-3
75. Thornton MM, Shrestha R, Wei Y, Thornton PE, Kao S, Wilson BE. DaymetDaymet: Daily Surface Weather Data on a 1-Km Grid for North America, Version 4. 2020. doi:10.3334/ORNLDAAC/1840.
76. Gent PR, Danabasoglu G, Donner LJ, et al. The Community Climate System Model Version 4. *J Climate*. 2011;24(19):4973-4991. doi:10.1175/2011JCLI4083.1
77. Raz-Yaseef N, Young-Robertson J, Rahn T, et al. Evapotranspiration across Plant Types and Geomorphological Units in Polygonal Arctic Tundra. *J Hydrol*. 2017;553(October):816-825. doi:10.1016/j.jhydrol.2017.08.036
78. Dengel S, Billesbach D, Torn M. NGEE Arctic CO2, CH4 and Energy Eddy-Covariance (EC) Flux Tower Auxiliary Measurements, Utqiagvik (Barrow), Alaska, 2012 - Ongoing. Next Generation Ecosystem Experiments Arctic Data Collection, Oak Ridge National Laboratory, U.S. Department of Energy, Oak Ridge, Tennessee, USA. 2020. doi:10.5440/1362279
79. Frampton A, Painter SL, Destouni G. Permafrost Degradation and Subsurface-Flow Changes Caused by Surface Warming Trends. *Hydrgeol J*. 2013;21(1):271-280. doi:10.1007/s10040-012-0938-z
80. McKenzie JM, Voss CI. Permafrost Thaw in a Nested Groundwater-Flow System. *Hydrgeol J*. 2013;21(1):299-316. doi:10.1007/s10040-012-0942-3
81. Sjöberg Y, Jan A, Painter SL, et al. Permafrost Promotes Shallow Groundwater Flow and Warmer Headwater Streams. *Water Resour Res*. 2021;57(2). doi:10.1029/2020WR027463
82. French, Hugh M. 2017. *The Periglacial Environment*. John Wiley & Sons, doi:10.1002/9781119132820.
83. Sannel AB, Hugelius KG, Jansson P, Kuhry P. Permafrost Warming in a Subarctic Peatland – Which Meteorological Controls Are Most Important? *Permafr Periglac Process*. 2016;27(2):177-188. doi:10.1002/ppp.1862
84. Zhang T, Stamnes K. Impact of Climatic Factors on the Active Layer and Permafrost at Barrow, Alaska. *Permafr Periglac Process*. 1998;9(3):229-246. doi:10.1002/(SICI)1099-1530(199807/09)9:3%3C229::AID-PPP286%3E3.0.CO;2-T
85. Burn CR, Lewkowicz AG, Alice Wilson M. Long-Term Field Measurements of Climate-Induced Thaw Subsidence above Ice Wedges on Hillslopes, Western Arctic Canada. *Permafr Periglac Process*. 2021;32(2):261-276. doi:10.1002/ppp.2113
86. Hinkel KM, Nelson FE. Spatial and Temporal Patterns of Active Layer Thickness at Circumpolar Active Layer Monitoring (CALM) Sites in Northern Alaska, 1995–2000. *J Geophys Res Atmos*. 2003;108(D2). doi:10.1029/2001JD000927
87. Romanovsky VE, Sergueev DO, Osterkamp TE. Temporal Variations in the Active Layer and Near-Surface Permafrost Temperatures at the Long-Term Observatories in Northern Alaska. *Permafrost*. 2003;1(2):989-994.
88. Lafrenière MJ, Lamoureux SF. Effects of changing permafrost conditions on hydrological processes and fluvial fluxes. *Earth Sci Rev*. 2019;191:212-223. doi:10.1016/j.earscirev.2019.02.018
89. Hamm A, Frampton A. Impact of Lateral Groundwater Flow on Hydrothermal Conditions of the Active Layer in a High-Arctic Hillslope Setting. *Cryosphere*. 2021;15(10):4853-4871. doi:10.5194/tc-15-4853-2021
90. Kane DL, Hinkel KM, Goering DJ, Hinzman LD, Outcalt SI. Non-Conductive Heat Transfer Associated with Frozen Soils. *Global Planet Change*, Inference of Climate Change from Geothermal Data. 2001;29(3):275-292. doi:10.1016/S0921-8181(01)00095-9
91. Zwieback S, Westermann S, Langer M, Boike J, Marsh P, Berg A. Improving Permafrost Modeling by Assimilating Remotely Sensed Soil Moisture. *Water Resour Res*. 2019;55(3):1814-1832. doi:10.1029/2018WR023247

SUPPORTING INFORMATION

Additional supporting information may be found in the online version of the article at the publisher's website.

How to cite this article: Jan A. Modeling the role of lateral surface flow in low-relief polygonal tundra. *Permafrost and Periglac Process*. 2022;33(3):214-225. doi:10.1002/ppp.2145